THE JOURNAL OF BIOLOGICAL CHEMISTRY VOL. 290, NO. 10, pp. 6179–6190, March 6, 2015

Modulation of Plasma Membrane Ca^{2+}-ATPase by Neutral Phospholipids

*EFFECT OF THE MICELLE-VESICLE TRANSITION AND THE BILAYER THICKNESS**

Received for publication, May 30, 2014, and in revised form, October 29, 2014 Published, JBC Papers in Press, January 20, 2015, DOI 10.1074/jbc.M114.585828

María Florencia Pignataro[‡], Martín M. Dodes-Traian[‡], F. Luis González-Flecha[‡], Mauricio Sica[§], Irene C. Mangialavori[‡1], and Juan Pablo F. C. Rossi[‡]

From the [‡]Instituto de Química y Fisicoquímica Biológicas, Facultad de Farmacia y Bioquímica, Universidad de Buenos Aires, CONICET, Junín 956 (1113) Buenos Aires, Argentina and the [§]Laboratorio de Bioenergías, IEDS, CONICET Centro Atómico Bariloche, E. Bustillo 9,500 (8400), San Carlos de Bariloche, Río Negro, Argentina

Background: Membrane proteins require phospholipids to be biologically active.
Results: An increase of phosphatidylcholine/detergent molar ratio leads to a biphasic behavior of the PMCA Ca^{2+}-ATPase activity, whose maximum depends on phosphatidylcholine characteristics.
Conclusion: The optimum hydrophobic thickness for PMCA structure and Ca^{2+}-ATPase activity is about 24 Å.
Significance: Differential modulation by neutral phospholipids could be a general mechanism for regulating membrane protein function.

The effects of lipids on membrane proteins are likely to be complex and unique for each membrane protein. Here we studied different detergent/phosphatidylcholine reconstitution media and tested their effects on plasma membrane Ca^{2+} pump (PMCA). We found that Ca^{2+}-ATPase activity shows a biphasic behavior with respect to the detergent/phosphatidylcholine ratio. Moreover, the maximal Ca^{2+}-ATPase activity largely depends on the length and the unsaturation degree of the hydrocarbon chain. Using static light scattering and fluorescence correlation spectroscopy, we monitored the changes in hydrodynamic radius of detergent/phosphatidylcholine particles during the micelle-vesicle transition. We found that, when PMCA is reconstituted in mixed micelles, neutral phospholipids increase the enzyme turnover. The biophysical changes associated with the transition from mixed micelles to bicelles increase the time of residence of the phosphorylated intermediate (*E*P), decreasing the enzyme turnover. Molecular dynamics simulations analysis of the interactions between PMCA and the phospholipid bilayer in which it is embedded show that in the 1,2-dioleoyl-*sn*-glycero-3-phosphocholine bilayer, charged residues of the protein are trapped in the hydrophobic core. Conversely, in the 1,2-dimyristoyl-*sn*-glycero-3-phosphocholine bilayer, the overall hydrophobic-hydrophilic requirements of the protein surface are fulfilled the best, reducing the thermodynamic cost of exposing charged residues to the hydrophobic core. The apparent mismatch produced by a 1,2-dioleoyl-*sn*-glycero-3-phosphocholine thicker bilayer could be a structural foundation to explain its functional effect on PMCA.

The superfamily of P-type ATPases encompasses a large group of enzymes responsible for active transport of cations across the cell membrane. They use the hydrolysis of ATP as a source of energy and share in common the formation of an acid-stable phosphorylated intermediate aspartyl-phosphate in their reaction cycle. The plasma membrane calcium pump (PMCA)[2] is a P-type ATPase that participates as an integral part of the Ca^{2+} signaling mechanism from eukaryotic cells (1) and is thus a crucial component of cell function. The enzyme exists in two main conformations, E_1 and E_2, according to the current kinetic model. Intracellular Ca^{2+} binds to high affinity sites in the E_1 conformation, and this event leads to phosphorylation by ATP with formation of E_1P. Subsequently, a conformational transition occurs (E_2P), and the Ca^{2+} is released to the extracellular medium from low affinity sites, followed by hydrolysis of the phosphoenzyme to E_2 and a new conformational transition to E_1 (2).

P-type ATPases and other integral membrane proteins operate surrounded by a lipid bilayer. The composition of the lipid environment is typically complex and dynamic. Importantly, its characteristics should support at least a close optimal protein functioning. Integral membrane proteins and lipids interact in two different major ways: (i) interactions of lipid molecules at membrane protein-specific sites (3, 4) and (ii) interactions of phospholipids with the transmembrane surface of membrane proteins at nonspecific sites. The structure of these phospholipids could be important in determining the conformation of

* This work was supported by Agencia Nacional de Promoción Científica y Tecnológica, CONICET, and Universidad de Buenos Aires, Ciencia y Técnica.
[1] To whom correspondence should be addressed: Instituto de Química y Fisicoquímica Biológicas, Facultad de Farmacia y Bioquímica, Universidad de Buenos Aires, CONICET, Junín 956 (1113) Buenos Aires, Argentina. E-mail: irenem@qb.ffyb.uba.ar.

[2] The abbreviations used are: PMCA, plasma membrane calcium pump; CaM, calmodulin; $C_{12}E_{10}$, polyoxyethylene(10)dodecyl ether; FCS, fluorescence correlation spectroscopy; PC, phosphatidylcholine; DMPC, 1,2-dimyristoyl-*sn*-glycero-3-phosphocholine; DOPC, 1,2-dioleoyl-*sn*-glycero-3-phosphocholine; DLPC, 1,2-dilauroyl-*sn*-glycero-3-phosphocholine; DPPC, 1,2-dipalmitoyl-*sn*-glycero-3-phosphocholine; (di14:1)PC, 1,2-dimyristoleoyl-*sn*-glycero-3-phosphocholine; (di16:1)PC, 1,2-dipalmitoleoyl-*sn*-glycero-3-phosphocholine; MD, molecular dynamics; [^{125}I]TID-PC/16, 1-palmitoyl-2-(9-(2′-[^{125}I]iodo-4′-(trifluoromethyldiazirinyl)-benzyloxycarbonyl)-nonaoyl)-*sn*-glycero-3-phosphocholine; Rho-DPPE, 1,2-dipalmitoyl-*sn*-glycero-3-phosphoethanolamine-*N*-(lissaminerhodamine B sulfonyl).

the protein and hence its activity (5). To conduct different experiments, membrane proteins can be purified and reconstituted in phospholipid - detergent mixed micelles. In this system, the hydrophobic regions of the protein are solvated with the nonpolar groups available in a dispersed lipid solution. Particularly, PMCA could be purified from detergent-solubilized erythrocyte plasma membranes and reconstituted in phospholipid-detergent mixed micelles. In these conditions, the purified enzyme preserves the biochemical properties of the PMCA in the erythrocyte membrane (6). This finding has validated the use of these micellar preparations for structural and functional studies (7).

It has been previously demonstrated that PMCA activity and also stability are influenced by phospholipids (8). Acidic phospholipids act as specific activators by increasing the apparent affinity for Ca^{2+} and also the maximal activity (V_{max}) (9–11). Importantly, neutral phospholipids, typically phosphatidylcholines, are essential for the enzyme basal activity. Recently, we employed a phospholipid analog, [^{125}I]TID-PC/16, to assess different transmembrane conformations of PMCA from the study of lipid-protein interaction (12). Using the same experimental approach and kinetic measurements, we proposed a model for the PMCA cycle that included structural information about the transmembrane domain and its interaction with neutral phospholipids (13). Our results showed that the amount of PMCA annular lipids (*i.e.* the layer(s) of lipid surrounding the transmembrane domain of the protein) changes dynamically during the pump reaction cycle.

A great number of studies have thoroughly characterized the effect of the lipid environment on the activity of purified preparations of different P-ATPases. Nonetheless, only a few of them have addressed the importance of the phospholipid proportion over the ATPase activity when working within these micellar reconstitution systems. It has recently been reported that an increasing phosphatidylcholine molar ratio in mixed micelles exerts a positive modulatory effect over the PMCA Ca^{2+}-ATPase activity, regardless of the total concentration of the individual amphiphiles (14). It can be hypothesized that the different reconstitution systems may exert their effects by favoring or impairing any of the PMCA reaction intermediates. However, a more detailed analysis of this effect on the whole spectrum of phospholipid/detergent molar ratio is yet to be performed. Moreover, it has been shown for other P-type ATPases that the hydrophobic thickness of the surrounding bilayer exerts an effect over the enzyme activity (5, 15, 16). Because the hydrophobic thickness of the lipid bilayer is expected to match the hydrophobic thicknesses of the proteins inserted in that membrane (17), the use of phospholipids with different chain lengths in the micelle may shed light on the elucidation of the optimal conditions for measuring PMCA activity.

In this work, we studied the effect of an increasing phospholipid molar ratio on PMCA Ca^{2+}-ATPase activity. To this aim, we reconstituted PMCA in mixed micelles with different $C_{12}E_{10}$/PC ratio and different PC acyl chains. We employed static light scattering and fluorescence correlation spectroscopy (FCS) to characterize the micelle-vesicle transition of the different reconstitution systems. We also determined the levels of PMCA phosphorylated intermediates to functionally describe the effects exerted not only by the phospholipid molar ratio in the micelle but also by the different phospholipid chain lengths. Finally, molecular dynamics simulations were carried out in the presence of bilayers composed of 1,2-dimyristoyl-*sn*-glycero-3-phosphocholine (DMPC) or 1,2-dioleoyl-*sn*-glycero-3-phosphocholine (DOPC) to explore the effect of the thickness of the transmembrane domain on the Ca^{2+} pump activity.

EXPERIMENTAL PROCEDURES

Reagents—All chemicals used in this work were of analytical grade and purchased mostly from Sigma-Aldrich. All of the phospholipids used in this work were purchased from Avanti Polar Lipids and stored as chloroform solution (when necessary). Phospholipids used in this study were 1,2-dilauroyl-*sn*-glycero-3-phosphocholine (DLPC), DMPC, 1,2-dipalmitoyl-*sn*-glycero-3-phosphocholine (DPPC), 1,2-dimyristoleoyl-*sn*-glycero-3-phosphocholine ((di14:1)PC), 1,2-dipalmitoleoyl-*sn*-glycero-3-phosphocholine ((di16:1)-PC), DOPC, and 1,2-dipalmitoyl-*sn*-glycero-3-phosphoethanolamine-*N*-(lissaminerhodamine B sulfonyl) (Rho-DPPE). [γ-^{32}P]Adenosine 5′-triphosphate was obtained from Perkin-Elmer Life Sciences. Recently drawn human blood for the isolation of PMCA was obtained from the Hematology Section of Fundosol Foundation (Argentina). Blood donation in Argentina is voluntary, and therefore the donor provides informed consent for the donation of blood and for its subsequent legitimate use by the transfusion service.

Purification of Plasma Membrane Calcium Pump from Human Erythrocytes—PMCA4 is the predominant isoform of human erythrocytes, which contain about 80% of this isoform and 20% PMCA1 (18). PMCA was isolated from CaM-depleted erythrocyte membranes by affinity chromatography in a calmodulin-agarose column as described previously (19) with some modifications. Purified PMCA was reconstituted in buffer containing 20% (m/v) glycerol, 0.005% $C_{12}E_{10}$, 120 mM KCl, 1 mM $MgCl_2$, 10 mM MOPS-K (pH 7.4 at 4 °C), 2 mM EGTA, 2 mM dithiothreitol (DTT) and stored under liquid nitrogen until use. Protein concentration after purification was about 10 μg/ml. No phospholipids were added at any step along the purification procedure. The performed procedure ensures almost complete delipidation of PMCA. The kinetic properties and regulatory characteristics of the enzyme are preserved by this purification procedure (11, 19). Free calcium concentration was calculated by the Max Chelator program and controlled with an Orion electrode (OR-9720BNWP).

Phospholipid Quantification—Phospholipid concentration was measured according to Chen *et al.* (20) with some modifications. Samples and standards containing 10–100 nmol of phosphorus were dried by heating at 100 °C. Mineralization was carried out by adding 0.1 ml of HNO_3, 0.9 ml of $HClO_4$ and incubating at 190 °C for 30 min. Inorganic phosphate was determined by the Fiske and Subbarow method (21).

Preparation of Phospholipid-detergent Mixed Micelles—Different amounts of phospholipids were solubilized with chloroform. The solvent was then evaporated under reduced pressure. The dried lipid film was solubilized by the addition of an adequate amount of $C_{12}E_{10}$ 1% (*i.e.* 1 g of $C_{12}E_{10}$ in 100 ml of water) to achieve a phospholipid/detergent molar ratio (X_{PC}) of 0.8,

followed by vigorous mixing and sonication above the transition temperature of each phospholipid. Phospholipid concentration was determined as described above. Mixtures with different phospholipid/detergent molar ratios were prepared by mixing the adequate amounts of phospholipid/$C_{12}E_{10}$ and $C_{12}E_{10}$ stock solutions. All amphiphilic mixtures were prepared with milli-Q water. Before sealing each tube, we removed most of the oxygen atmosphere from the sample by blowing a stream of nitrogen gas over the solution. These mixtures were not conserved for more than 7 days at −20 °C.

Measurement of Ca^{2+}-ATPase Activity—ATPase activity was measured by following the release of inorganic phosphate from ATP as described previously by Fiske and Subbarrow (20) or by measuring the [^{32}P]P_i released from [γ-^{32}P]ATP as described by Richards *et al.* (22). In each condition, the quantity of P_i released in the absence of calcium was subtracted from the P_i released in its presence. The reaction medium consisted of 120 mM KCl, 30 mM MOPS-K (pH 7.2 at 37 °C), 3.75 mM $MgCl_2$, 1 mM EGTA, and enough $CaCl_2$ to give 100 μM final free [Ca^{2+}]. The $C_{12}E_{10}$ concentration was 120 μM, and an adequate amount of the phospholipid stock solutions was added to achieve the desired molar ratio (which can be expressed as X_{PC}). When necessary (as indicated in the experiment), A23187 ionophore was added to the previous reaction medium at the concentrations indicated in the figure. The reaction was started by the addition of ATP (final concentration of 2 mM for the non-radioactive assay and 30 μM for the radioactive ones). The experimental setup was adjusted to ensure that PMCA (7 nM) initial velocity conditions were met. Measurements were carried out at 37 °C (non-radioactive assay) or 25 °C (radioactive assay).

Measurement of Static Light Scattering—Micelle-vesicle transition was monitored at 37 °C in a 3 × 3 quartz cuvette by using a Jasco FP-6500 spectrofluorimeter equipped with a Jasco ETC-237T Peltier temperature controller. 90° light scattering was measured at 470 nm with a bandwidth of 3 nm for 120 s. Every sample was identical to the Ca^{2+}-ATPase activity medium, excluding PMCA.

FCS—Before making FCS measurements, samples were incubated 60 min at room temperature in the presence of 10 nM Rho-DPPE. The concentration of the probe provides an average of 0.1 fluorescent molecules/micelle to ensure an adequate signal/noise ratio of the diffusing particles. All FCS experiments were carried out at 25 °C. Experiments were performed with a confocal Olympus FV-1000 microscope with a 1.35 numerical aperture ×60 oil immersion objective. Calibration was performed by using a 50 nM solution of the protein BSA labeled with the fluorescent probe fluorescein isothiocyanate (BSA-FITC) in 0.1 M guanidine hydrochloride to prevent dimerization ($D = 63\ \mu m^2 \cdot s^{-1}$) (23). The samples were excited at 559 nm with a solid state laser at a nominal power of 8%. The detector was configured in pseudo-photon counting mode. The sampling frequency ranged from 10 to 50 kHz in order to ensure the best definition of the autocorrelation curves. Data acquisition took 120 s, and each sample was measured five times. Autocorrelation curves (24) were generated by using the equation,

$$G(\tau) = \frac{\langle \delta F(t) \cdot \delta F(t+\tau) \rangle}{\langle F(t) \rangle^2} \quad \text{(Eq. 1)}$$

where $\langle \delta F(t) \cdot \delta F(t+\tau) \rangle$ represents the fluctuation at time t, and τ represents a time lag. The obtained experimental autocorrelation function was fitted to a passive three-dimensional diffusion model,

$$G(\tau) = \frac{\gamma}{N}\left(1 + \frac{\tau}{\tau_D}\right)^{-1}\left(1 + \left(\frac{w_0}{z_0}\right)^2 \cdot \frac{\tau}{\tau_D}\right)^{-\frac{1}{2}} \quad \text{(Eq. 2)}$$

where N represents the mean number of molecules in the observation volume, w_0 and z_0 represent radial and axial waist of the observation volume, and γ is a geometric correction factor for the effective volume with a value of $1/\sqrt{8}$ for a Gaussian detection profile. Mean residence time of a particle in the observation volume is represented by τ_D. The diffusion coefficient D of a molecule can be calculated from τ_D.

$$\tau_D = \frac{{w_0}^2}{4D} \quad \text{(Eq. 3)}$$

Considering a spherical particle, the hydrodynamic radius can be calculated using the Stokes-Einstein equation.

$$R_H = \frac{kT}{6\pi D\eta} \quad \text{(Eq. 4)}$$

Determination of Phosphorylated Intermediates—The phosphorylated intermediates (*E*P) were measured as the amount of acid-stable ^{32}P incorporated into the enzyme (0.9 μg/ml), according to the method described by Echarte *et al.* (25). The phosphorylation was measured at 25 °C in a medium containing 30 mM MOPS-K (pH 7.4 at 4 °C), 120 mM KCl, 3.75 mM $MgCl_2$, 2 mM EGTA, 30 μM [γ-^{32}P]ATP, 75 μM $LaCl_3$ (where indicated), and enough $CaCl_2$ to obtain a 100 μM final free calcium concentration. The $C_{12}E_{10}$ concentration was kept constant at 120 μM. The phospholipid concentration corresponded to the molar ratio of the activity assay. The reaction was started by the addition of [γ-^{32}P]ATP under vigorous stirring, and after 30 s, it was stopped with an ice-cold solution of TCA (10% (w/v) final concentration). The tubes were centrifuged at 10,000 rpm for 5 min at 4 °C. The samples were then washed once with 7% TCA, 150 mM H_3PO_4 and once with double-distilled water and processed for SDS-PAGE. For this purpose, the pellets were dissolved in a medium containing 150 mM Tris-HCl (pH 6.5 at 14 °C), 5% SDS, 5% DTT, 10% glycerol, and bromphenol blue (sample buffer). Electrophoresis was performed at pH 6.5 (14 °C) in a 7.5% polyacrylamide gel. The reservoir buffer was 0.1 M sodium phosphate, pH 6.3, with 0.1% SDS. Migration of the sample components took place at 14 °C with 60 mA until the tracking dye reached a distance about 10 cm from the top of the gel. Gels were stained, dried, and exposed to a Storage Phospho-Screen (Amersham Biosciences). Unsaturated autoradiograms were scanned with the Storm Molecular Image System, and stained gels were scanned with an HP Scanjet G2410 scanner. Analysis of the images was performed with GelPro Analyzer. *E*P quantification was achieved as described by Echarte *et al.* (25).

Molecular Dynamics Simulations of PMCAHS—The structure of PMCA covering residues 1–1056 was obtained by homology modeling against the structure of SERCA (Protein Data Bank code 1T5S) using MODELLER version 9.14 and the alignment published previously (26). Remaining C-end residues (positions 1057–1205) were not included in the model. The protein was placed in a triclinic box and embedded in a membrane composed of DMPC or DOPC molecules. Both membranes were previously equilibrated and originally consisted of 512 lipid molecules. Simulations were performed in GROMACS version 4.5.4 (27) using the G53a6 force field. To embed the protein, the InflateGRO2 package was used (28), and the final membranes were composed of 454 DMPC or 467 DOPC molecules. The systems were hydrated with simple point charge water molecules, and sodium and chlorine ions were added until a 0.15 M final concentration. After steepest descent minimization, both systems were subjected to simulations with the protein CA atoms position-restrained at 313 K and with 2-fs time steps. The first 2 ns were performed under NVT (where "N" is the constant particle number, "V" is volume, and "T" is temperature) conditions and then to a further 2 ns under NPT (where "P" is pressure) conditions. Then the systems were subjected to 5 ns of unconstrained molecular dynamics simulations at 1 bar with weak temperature coupling. All hydrogen atoms were considered explicitly, and protein covalent bonds were constrained using LINCS (29).

Data Analysis—Data presented in this work are representative of three independent experiments. Activity measurements were performed in triplicate. Equations were fitted to the experimental data using a non-linear regression procedure based on the Gauss-Newton algorithm. Statistical analyses were performed using Excel software (Microsoft) and Sigma Plot for Windows, the latter being able to provide not only the best fitting values of the parameters but also their S.E. values. Statistical significance was determined by Student's *t* test.

RESULTS

Increasing X_{PC} of Neutral Phospholipids Leads to a Biphasic Behavior of the Ca^{2+}-ATPase Activity—In order to study the effect of mixed micelle composition on PMCA activity, the pump was reconstituted in systems with increasing PC/$C_{12}E_{10}$ ratios and different PC acyl chain length and degree of unsaturation. The $C_{12}E_{10}$ concentration was fixed at 120 μM, given that the change in $C_{12}E_{10}$ concentration might itself alter the activity.

Fig. 1*A* shows Ca^{2+}-ATPase activity as a function of molar fraction (X_{PC}) of DLPC, DMPC, and DPPC. Fig. 1*B* shows Ca^{2+}-ATPase activity as a function of X_{PC} using monounsaturated PCs: (di14:1)PC, (di16:1)PC, and DOPC. In every condition, PMCA activity showed a biphasic behavior. At first, ATPase activity increased with increasing X_{PC}, reaching a maximal value, and decreased afterward. However, some important differences were observed among the different phospholipids assayed in the activation phase. Therefore, to obtain quantitative information on this phenomenon, we employed the mechanistic model proposed by Dodes Traian *et al.* (14).

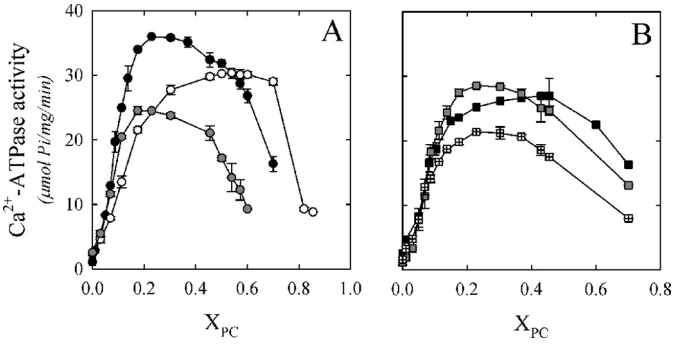

FIGURE 1. **PMCA Ca^{2+}-ATPase activity as a function of the molar fraction (X_{PC}) of different phospholipids.** *A*, Ca^{2+}-ATPase activity as a function of the molar fraction (X_{PC}) of DLPC (*white circles*), DMPC (*black circles*), and DPPC (*gray circles*). *B*, Ca^{2+}-ATPase activity as a function of X_{PC} of (di14:1)PC (*black* squares), (di16:1)PC (*gray squares*), and DOPC (*squares with crosses*). The $C_{12}E_{10}$ concentration was kept constant at 120.0 μM, and ATPase activity measurement was performed as described under "Experimental Procedures." The values shown are the mean ± S.E. (*error bars*) of at least three independent experiments performed in triplicate.

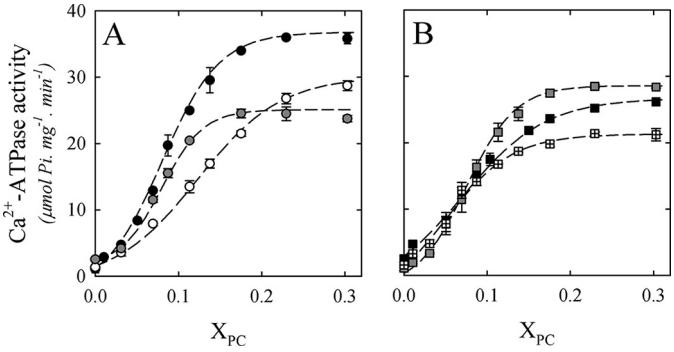

FIGURE 2. **Fitting of the two-state model to the activation phase of Ca^{2+}-ATPase activity.** *A*, Ca^{2+}-ATPase activity as a function of X_{PC} of DLPC (*white circles*), DMPC (*black circles*), and DPPC (*gray circles*). *B*, Ca^{2+}-ATPase activity as a function of X_{PC} of (di14:1)PC (*black squares*); (di16:1)PC (*gray squares*), and DOPC (*squares with crosses*). *Dotted lines* in *A* and *B* correspond to the fitting of Equation 5 to the experimental data between X_{PC} 0 and 0.3 for all of the phospholipids assayed. The best fitting parameters are shown in Table 1. The values shown are mean ± S.E. (*error bars*) of at least three independent experiments.

Activation of Ca^{2+}-ATPase Activity by Neutral Phospholipids—The behavior observed in Fig. 1 for the PMCA Ca^{2+}-ATPase activity as a function of X_{PC} (until X_{PC} = 0.3) was observed first in DPPC-$C_{12}E_{10}$ mixtures (14). In this work, the authors postulated a two-stage mechanistic model explaining the modulation of protein activity based on the exchange among non-structural amphiphiles at the hydrophobic transmembrane surface and a lipid-induced conformational change. Equation 5 describes the minimal model proposed by the authors,

$$A = \frac{A_1 - A_0}{1 + e^{-c_x(X - X_{0.5})}} + A_0 \qquad \text{(Eq. 5)}$$

where $X_{0.5}$ represents the phospholipid molar fraction that gives half-activation effect, c_x is the empirical cooperativity coefficient related to the maximal slope, and A_0 and A_1 are the lower and upper asymptotes of the equation, respectively. *Dotted lines* in Fig. 2, *A* and *B*, correspond to the global fitting of Equation 5 to the experimental data, between X_{PC} of 0 and 0.3. The minimal model accurately described our data in the men-

tioned range for all of the phospholipids assayed. The best fitting parameter values are shown in Table 1. We obtained different maximal levels of Ca^{2+}-ATPase activity (A_1) for every $PC/C_{12}E_{10}$ reconstitution system. Interestingly, PMCA maximal activity was obtained for the enzyme reconstituted in $DMPC/C_{12}E_{10}$ mixed micelles. On the contrary, the lower activity was obtained in the presence of $DOPC/C_{12}E_{10}$ mixed micelles. If we focus on unsaturated phospholipids, the maximal PMCA activity was observed with (16:1) PC. These findings demonstrate that the maximal PMCA Ca^{2+}-ATPase activity largely depends on the length and also on the unsaturation degree of each PC assayed. We also found that the X_{PC} that gives a half-activation effect ($X_{0.5}$) was similar for all lipids assayed except for DLPC, for which a higher proportion of lipid molecules in the mixed micelle was necessary to reach the coverage of the transmembrane hydrophobic surface of PMCA that leads to the maximal Ca^{2+}-ATPase activity. On the other hand, the c_x parameter takes its maximal value for DPPC and is minimal for DLPC and (di14:1)PC. This parameter gives a combined measure of both the affinity of a given phospholipid for the hydrophobic transmembrane surface of the protein and the cooperative effect of this phospholipid activating the enzyme (14). Thus, the high value of c_x observed for DPPC indicates that this phospholipid is a more efficient activator of PMCA (*i.e.* small changes in its proportion in the micelles (or in the membrane) can produce a significant change in the enzyme activity). A similar mechanism could operate with other lipids and membrane proteins, constituting a key event in regulating the function of membrane protein *in vivo*.

TABLE 1

Parameters obtained for PMCA after fitting Equation 5 to the experimental data of Fig. 2

$X_{0.5}$ represents the phospholipid molar fraction that gives half-activation effect, c_x is the empirical cooperativity coefficient related to the maximal slope, and A_1 is the upper asymptote of Equation 5. The global fitting was performed assuming that the activity of PMCA in the absence of added phospholipids is equal for all samples, obtaining a value of 1.7 ± 0.2.

Phospholipid	A_1	$X_{0.5}$	c_x
DLPC	30.2 ± 0.5	0.11 ± 0.01	18 ± 1
DMPC	36.0 ± 0.4	0.08 ± 0.01	31 ± 2
DPPC	24.4 ± 0.4	0.07 ± 0.01	41 ± 4
(di14:1)PC	26.7 ± 0.3	0.05 ± 0.01	19 ± 2
(di16:1)PC	28.4 ± 0.3	0.08 ± 0.01	35 ± 3
DOPC	21.1 ± 0.3	0.06 ± 0.01	27 ± 3

Taken together, these findings validate the use of Equation 5 in different reconstitution systems and allowed us to obtain a set of parameters that could shed light on the mechanism underlying the activation process. Nevertheless, the mentioned model did not predict the behavior observed for PMCA Ca^{2+}-ATPase activity in the whole range of X_{PC} values assayed (Fig. 1).

The Decrease in Ca^{2+}-ATPase Activity at High X_{PC} Is Associated with a Micelle-Vesicle Transition—The vesicle to micelle transition was extensively studied using different techniques, and it has been reported that it may occur in the detergent/phospholipid ratio assayed here (30–33). These studies suggest that this process can be interpreted with a three-step molecular model and that it is a reversible process (*i.e.* detergent micelles can be enriched with phospholipids, producing the inverse transition) (34, 35). To determine whether the decrease in

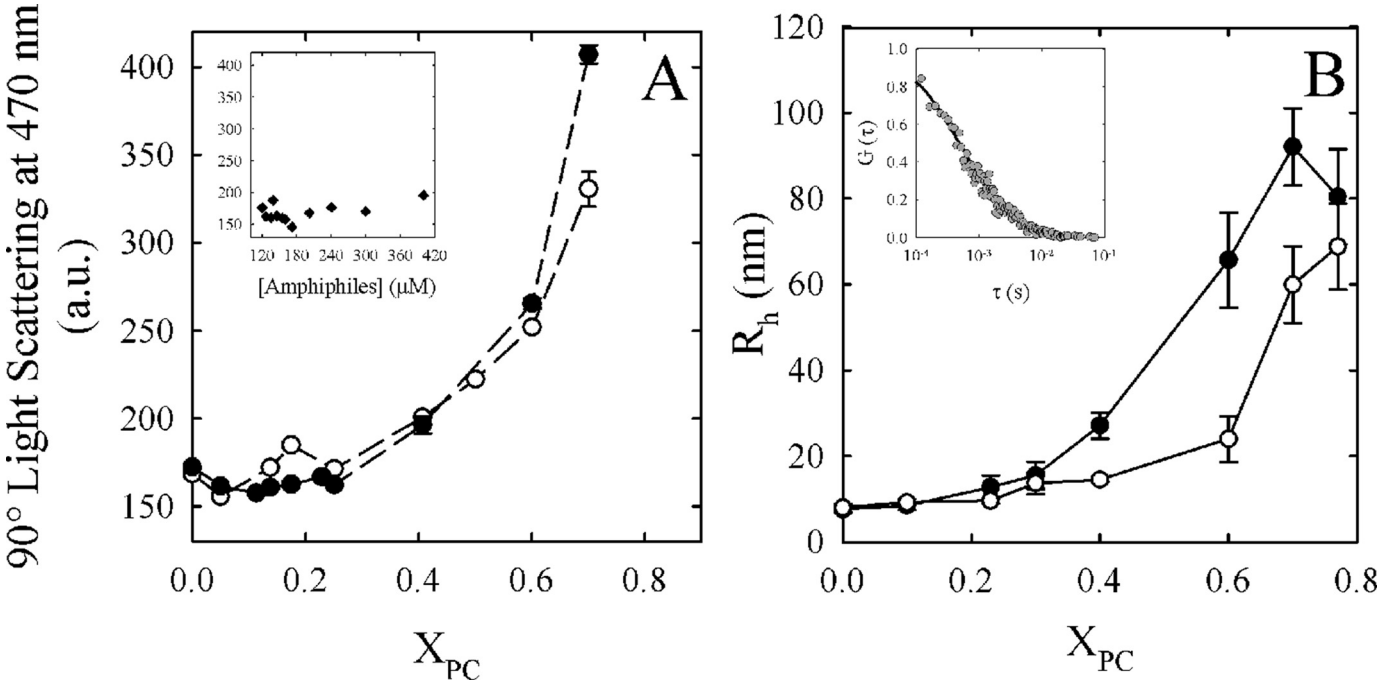

FIGURE 3. **Micelle-vesicle transition of $C_{12}E_{10}$/DLPC and $C_{12}E_{10}$/DMPC mixtures.** *A*, 90° light scattering (470 nm) expressed in arbitrary units (*a.u.*) as a function of X_{PC} for $C_{12}E_{10}$/DLPC (*white circles*) and $C_{12}E_{10}$/DMPC (*black circles*) mixtures in the same conditions in which the Ca^{2+}-ATPase activity was determined in Fig. 1*A*. No enzyme was added in the mixture. *Inset*, 90° light scattering (470 nm) as a function of $C_{12}E_{10}$ concentration (in the absence of DMPC or DLPC). *B*, hydrodynamic radius (R_H) of the micelles/vesicles as a function of X_{DLPC} (*white circles*) and X_{DMPC} (*black circles*), in the same conditions in which the Ca^{2+}-ATPase activity was determined in Fig. 1*A*. No enzyme was added in the mixture. *Inset*, normalized experimental autocorrelation curve obtained at $X_{DMPC} = 0.25$. By fitting a three-dimensional diffusion model (Equation 2) to these experimental data, we obtained a characteristic residence time (τ_D) of the particles diffusing through the observation volume. The residence time can be related to the diffusion coefficient D (Equation 3) and finally with the R_H (Equation 4) of the fluorescent particles. The values shown are the mean ± S.E. (*error bars*) of at least three independent experiments performed in triplicate.

Ca^{2+}-ATPase activity observed in Fig. 1 is due to a micelle-vesicle transition, we employed static light scattering and FCS on $C_{12}E_{10}$/DMPC and $C_{12}E_{10}$/DLPC mixtures. The latter was selected due to its differential behavior, in the decreasing phase, observed in Fig. 1. On the other hand, $C_{12}E_{10}$/DMPC mixtures were selected due to its representative behavior, with respect to the other amphiphilic systems assayed. Fig. 3*A* shows 90° light scattering (470 nm) for $C_{12}E_{10}$/DLPC and $C_{12}E_{10}$/DMPC mixtures at the same conditions in which the Ca^{2+}-ATPase activity was determined in Fig. 1*A* but in the absence of the enzyme. In both systems, there was a rise in the scattering starting from $X_{PC} = 0.40$, whereas the maximum value (at $X_{PC} = 0.70$) was lower in the $C_{12}E_{10}$/DLPC mixture. The observed rise in light scattering could be produced by an increase in the total amount of particles in the system. To discard this possibility, we included a set of conditions in which the final concentrations of amphiphiles were the same as the ones needed for every molar ratio used in Fig. 3*A* but in the absence of phospholipids (Fig. 3*A*, *inset*). No significant differences in scattering were observed between any of these conditions, showing that the increase in light scattering is produced by intrinsic differences in particle size and/or shape associated with $X_{PC.}$ These results demonstrate that the micelle-vesicle transition appears to occur at about $X_{PC} = 0.40$ in both mixtures. However, the size and/or shape of the particles observed at $X_{PC} = 0.7$ is different for $C_{12}E_{10}$/DLPC and $C_{12}E_{10}$/DMPC mixtures.

In order to further characterize the observed differences in particle size and also to link this phenomenon with the decreasing phase of Ca^{2+}-ATPase activity observed at higher X_{PC}, we employed fluorescence correlation spectroscopy (24) in $C_{12}E_{10}$/DLPC and $C_{12}E_{10}$/DMPC mixtures. FCS is based on fluorescence intensity fluctuations that take place in a very small observation volume, typically a few fl. The analysis of these fluctuations allowed us to determine the diffusion coefficient (D) of the hydrodynamic particle from which the hydrodynamic radius (R_H) can be obtained from Equation 4. In our experimental approach, the fluorescent phospholipid analog (Rho-DPPE) was incorporated into the amphiphilic system in order to obtain the diffusion coefficient of the micelles/vesicles. The *inset* from Fig. 3*B* shows a typical experimental autocorrelation curve obtained from these systems and the corresponding fit to a three-dimensional diffusion model.

Fig. 3*B* shows that the particle's R_H started to increase from about $X_{DMPC} = 0.3$ and $X_{DLPC} = 0.6$. These results show that although there is a transition taking place in the X_{PC} ranges assayed, the rise in size appears to start at higher X_{PC} in $C_{12}E_{10}$/DLPC mixtures. Moreover, we also found a different size at $X_{PC} = 0.70$ for both of the mixtures. These results are consistent with the stable Ca^{2+}-ATPase activity observed at $X_{DLPC} = 0.70$. As we have previously demonstrated, before the transition, the mechanistic model (Equation 5) predicts the behavior of Ca^{2+}-ATPase activity as a function of X_{PC}. In these conditions, the average size of the particles is nearly constant (Fig. 3*B*). Next, as the particle size increases, the Ca^{2+}-ATPase activity decreases.

To explain the decrease in Ca^{2+}-ATPase activity during the micelle-vesicle transition, we proposed the following hypotheses: (i) the enzyme is inserted in a vesicle in a way that may pump calcium toward the lumen of the vesicle, leading to the cation accumulation that would finally inhibit transport and ATPase activity; (ii) the enzyme is inserted in a vesicle with its catalytic site hidden from the substrates; (iii) the enzyme is less stable and tends to be inactivated; or (iv) the PMCA catalytic cycle is affected by the biophysical changes in the amphiphilic environment.

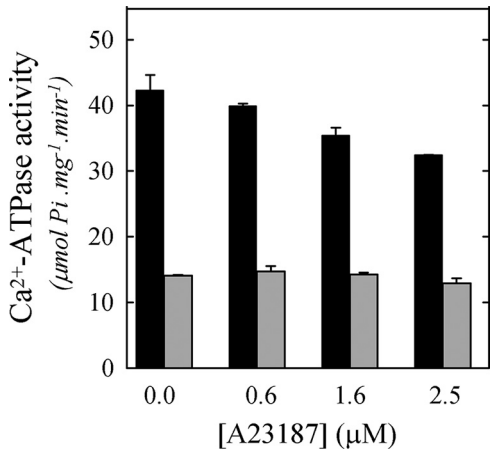

FIGURE 4. **Effect of a calcium ionophore on Ca^{2+}-ATPase activity.** Shown is Ca^{2+}-ATPase activity when PMCA was reconstituted at $X_{DMPC} = 0.25$ (*gray*) or 0.70 (*black*) and in the presence of increasing A23187 concentrations. The Ca^{2+}-ATPase activity measurement was performed as indicated under "Experimental Procedures." The values shown are mean ± S.E. (*error bars*) of two independent experiments performed in triplicate.

Ca^{2+}-ATPase Activity Does Not Recover in the Presence of a Ca^{2+} Ionophore—To address the first possibility, we measured the Ca^{2+}-ATPase activity of PMCA reconstituted in $C_{12}E_{10}$/DMPC mixtures in the presence of the calcium ionophore A23187. It is known that A23187 forms complexes with divalent cations and that it presents a particular high affinity for Ca^{2+} (36). These complexes go across the biological membranes, allowing the cation release (37). As a consequence, if the inhibition in the Ca^{2+}-ATPase activity is due to the vesicle filling with calcium, the addition of A23187 would reverse this effect (38).

We assayed two representative X_{DMPC} (0.25 and 0.70, pre- and post-transition, respectively). Fig. 4 shows the Ca^{2+}-ATPase activity of PMCA reconstituted in $X_{DMPC} = 0.25$ or 0.70 in the presence of different A23187 concentrations. The incorporation of A23187 did not prevent the decrease in Ca^{2+}-ATPase activity observed at $X_{DMPC} = 0.70$. There is a subtle A23187 concentration-dependent inhibitory effect observed at $X_{DMPC} = 0.25$ that can be attributed to a nonspecific effect on the enzyme (39). This result indicates that the decrease in Ca^{2+}-ATPase activity, observed after the micelle-vesicle transition, would not be due to the formation of closed vesicles that impair Ca^{2+} uptake.

The Amount of Active PMCA Is Similar Regardless the Existence of a Micelle-Vesicle Transition—PMCA forms an acid-stable phosphorylated intermediate (*E*P) during its reaction cycle. Lanthanum (La^{III}) is known to prevent the Mg^{2+}-dependent transition $E_1P \rightarrow E_2P$ (40, 41). Thus, the amount of *E*P obtained in the presence of La^{III} is usually considered as a valid calculation of the total active enzyme concentration (42). Therefore, to assess whether the lower Ca^{2+}-ATPase activity

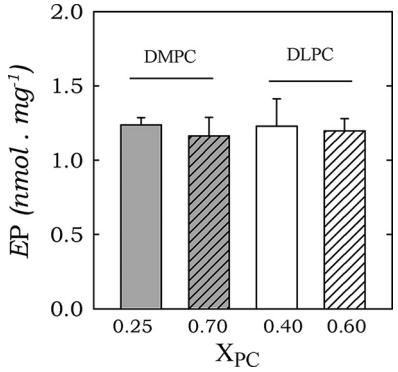

FIGURE 5. **Total phosphorylated intermediates (*EP*) of PMCA at optimal and inhibitory X_{DMPC} and X_{DLPC}.** PMCA was reconstituted in $X_{DMPC} = 0.25$ or 0.70 and $X_{DLPC} = 0.40$ or 0.70. Total phosphoenzyme formation from [γ-^{32}P]ATP was determined as described under "Experimental Procedures." The values shown are the mean ± S.E. (*error bars*) of two independent experiments performed in triplicate.

TABLE 2

Turnover (*kp* (s^{-1})) for PMCA in the presence of different phospholipid molar fractions

kp is the ratio between the Ca^{2+}-ATPase activity from Fig. 1A and the *Ep* values obtained in Fig. 5 in the presence of the X_{PC} shown in the table.

X_{PC}	*kp*
	s^{-1}
$X_{DLPC} = 0.40$	404 ± 34
$X_{DLPC} = 0.70$	403 ± 17
$X_{DMPC} = 0.25$	474 ± 11
$X_{DMPC} = 0.70$	233 ± 21
$X_{DOPC} = 0.30$	274 ± 19

found for reconstitution of PMCA at higher X_{PC} (Fig. 1) could be explained by a decrease in the concentration of active enzyme, we measured the total phosphoenzyme concentration from [γ-^{32}P]ATP in the presence of 50 μM La^{III}. PMCA was reconstituted in $C_{12}E_{10}$/DMPC and $C_{12}E_{10}$/DLPC mixtures at optimal (0.25 and 0.4, respectively) and higher molar ratios (0.70). Fig. 5 shows that there were not significant differences among the levels of *E*P in any of the conditions assayed. Consequently, the inhibition in Ca^{2+}-ATPase activity seen when PMCA was reconstituted in systems at higher molar ratios was not due to a decrease in the levels of active enzyme. Furthermore, this result also rules out the possibility that impairment in substrate or cofactor accessibility could lead to the decrease in PMCA activity.

The Observed Differences in Ca^{2+}-ATPase Activity Are Due to a Decline in PMCA Turnover—Once we have determined that the active enzyme concentration was the same for all of the conditions previously assayed (Fig. 5), we calculated the turnover (*kp*) of PMCA when the enzyme was reconstituted in $C_{12}E_{10}$/DMPC and $C_{12}E_{10}$/DLPC mixtures at optimal and higher molar ratios. Table 2 shows the *kp* values calculated as the ratio between the Ca^{2+}-ATPase activity from Fig. 1 and the amounts of active PMCA (*Ep* values obtained in Fig. 5). There is a decrease in *kp* at $X_{DMPC} = 0.70$. This result suggests that the decrease in Ca^{2+}-ATPase activity observed in Fig. 1 for most of the phospholipids assayed was due to an increase in transit time.

As the mixture that leads to the lower Ca^{2+}-ATPase activity at optimal X_{PC} (Fig. 2), we calculated the enzyme *kp* when PMCA was reconstituted in $C_{12}E_{10}$/DOPC micelles at optimal

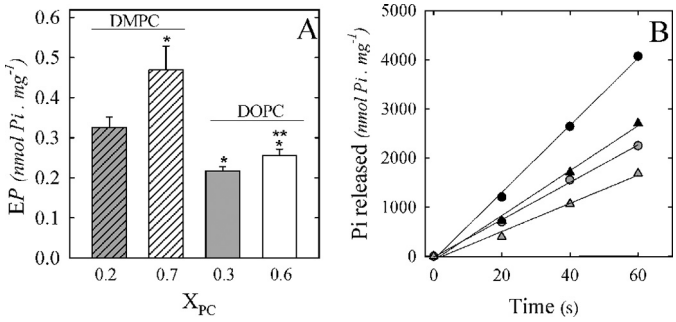

FIGURE 6. **Effect of PMCA reconstitution in $C_{12}E_{10}$/DMPC and $C_{12}E_{10}$/DOPC mixtures on the phosphorylated intermediates.** PMCA was reconstituted in $C_{12}E_{10}$/DMPC ($X_{DMPC} = 0.25$ and 0.7) or $C_{12}E_{10}$/DOPC ($X_{DOPC} = 0.3$ and 0.6), and steady-state *E*P levels (*A*) were determined in the same experimental conditions in which the Ca^{2+}-ATPase activity was determined in Fig. 1*A*, but ATP concentration was 30 μM ATP. *B*, Ca^{2+}-ATPase activity was calculated from the slope of P_i released as a function of time in the same experimental condition in which steady-state *E*P levels were determined. The values shown are mean ± S.E. (*error bars*) of at least three independent experiments performed in triplicate (*, $p < 0.0001$ with respect to $X_{DMPC} = 0.25$; **, $p < 0.05$ with respect to $X_{DOPC} = 0.3$).

$X_{DOPC} = 0.3$. Similarly, when reconstituted at $X_{DOPC} = 0.3$, the enzyme *kp* is lower than the one attained in $X_{DMPC} = 0.25$. Not surprisingly, the differences in the maximal activities obtained at the optimal X_{PC} for all of the phospholipids assayed (Table 1) may also be due to differences in the enzyme *kp*.

Effect of X_{PC} and Lipid Structure on the Time of Residence of the Phosphorylated Intermediates (EP)—It has been previously reported for SERCA that reconstitution into bilayers of phospholipids with different fatty acyl chains leads to different kinetics for ATPase activity due to effects on phosphorylation and dephosphorylation rates (43). Thus, to assess whether the differences in Ca^{2+}-ATPase activities obtained for the different phospholipids at optimal X_{PC} and the decrease in *kp* found for reconstitution at higher X_{PC} (Table 2) could be partially explained by alterations on the phosphorylated intermediates, we measured the levels of *E*P at steady state and at optimal and higher X_{PC} (Fig. 6*A*). DMPC and DOPC mixed micelles were chosen as models for this experiment because they showed maximal differences in Ca^{2+}-ATPase activity. For both phospholipids, there is an increase in the level of *E*P at higher X_{PC}. If we compare the *E*P levels attained at optimal X_{PC}, we observed that there is a decrease in this level in the presence of DOPC micelles.

Although the measurement of *E*P itself is relevant for the characterization of partial reactions of the enzyme cycle, we also decided to determine the time of residence in the phosphorylated intermediates in the previously assayed conditions. A residence time was defined as the actual time spent as a given intermediate during an isolated turnover (44). First, because the determination of the *E*P levels needed to be carried out in the presence of ATP 30 μM, we measured the Ca^{2+}-ATPase activity at the same experimental conditions (Fig. 6*B*). The PMCA specific activity was calculated from the slope of each curve (Table 3). There is a decrease in Ca^{2+}-ATPase activity in the presence of higher X_{PC}, and this drop is similar, for the two phospholipids assayed, to the observed behavior at 2 mM ATP (Fig. 1). Also, the Ca^{2+}-ATPase activity at optimal X_{DOPC} is about 40% lower than at optimal X_{DMPC}, also similar to the values obtained in

TABLE 3

PMCA residence time in *E*P (t(*E*P)) in the presence of different reconstitution systems

t(*EP*) is the ratio between *E*P levels in steady state and the Ca^{2+}-ATPase activity, which were determined in the same experimental conditions (30 μM ATP and 25 °C).

X_{PC}	*E*P level	Specific activity	*t*(*E*P)
	nmol P_i·mg^{-1}	*nmol P_i·mg^{-1}·s^{-1}*	*ms*
$X_{DMPC} = 0.25$	0.33 ± 0.03	68.2 ± 1.9	4.5 ± 0.2
$X_{DMPC} = 0.70$	0.47 ± 0.06	38.0 ± 1.1	11.9 ± 0.8
$X_{DOPC} = 0.30$	0.22 ± 0.01	45.6 ± 2.3	4.7 ± 0.1
$X_{DOPC} = 0.60$	0.26 ± 0.01	28.7 ± 2.1	7.9 ± 0.2

Fig. 1. These results indicate that the effects on the Ca^{2+}-ATPase activity produced by the different reconstitution systems are independent from the ATP concentrations assayed.

Table 3 shows the residence times calculated as the ratio between *E*P levels and the Ca^{2+}-ATPase activities. Results show that at higher X_{DMPC} and X_{DOPC}, the residence time of *E*P (*t*(*E*P)) increases (Table 3). The observed effects on *t*(*E*P) in the conditions mentioned above are in part due to an increase in *E*P levels (with respect to the levels observed at optimal X_{PC}). This can be due to an increase in the rate of formation of *E*P (higher rate of phosphorylation) or alternatively to a decrease in its breakdown (slower rate of dephosphorylation). Because the rate of the full cycle of the pump decreased in these systems, it is likely that the higher molar ratio effect on the *E*P is due to a slower rate of dephosphorylation. Conversely, there is not a significant difference in *t*(*E*P) between the two different phospholipids tested at the optimal X_{PC}. This finding suggests that the slower kinetics (decrease in *kp*) observed in the presence of DOPC (Table 2) at optimal X_{PC} may not be due to an effect on the phosphorylated intermediates but to any other step of the reaction cycle.

Molecular dynamics simulation of PMCA embedded in DMPC and DOPC bilayers. In order to analyze the structural changes that may take place when PMCA is exposed to different amphiphilic environments, we performed molecular dynamics (MD) simulations of PMCA inserted in DMPC or DOPC pure lipid bilayers. Because PMCA has not yet been crystallized, we used a recently described PMCA model that was based on a SERCA template (Protein Data Bank code 1T5S). Fig. 7 displays the average protein structure together with a brown surface representing the average positions of phosphorus atoms in the bilayer leaflets, calculated from MD simulation of PMCA in a bilayer of DMPC (*A*) or DOPC (*B*).

From our simulations, the estimated hydrophobic thicknesses of these bilayers are 24 and 29 Å, respectively. Along the simulations, the systems evolve to accommodate the upper layers of DMPC and DOPC to interact with the positive charges of Lys and Arg residues (in *cyan* and *blue sticks*). However, the lower layer of the DOPC bilayer leaves several positively charged groups within the hydrophobic core, namely Arg-80, Lys-365, Lys-828, Lys-897, and Lys-974. However, in the presence of DMPC membranes, these residues are located in a more polar environment interacting with phosphorus atoms or exposed to the solvent.

Fig. 7*B* shows the density graph of the polar heads and hydrophobic tails. For the densities of acyl chains of the DMPC and DOPC bilayer, no significant differences were observed. However, a decrease in the density of the headgroups only in the extracellular side of the DOPC membrane is revealed associated with the disruption of the membrane necessary to optimize the protein-membrane interactions, which is not observed with DMPC. Thus, the polar heads of the DMPC bilayer appear correctly packed, whereas in the case of the DOPC bilayer this may not be the case.

DISCUSSION

In this study, we demonstrated that neutral phospholipids modulate PMCA Ca^{2+}-ATPase activity. This modulation is highly dependent on the composition of the mixed micelles (X_{PC}) and also on the PC characteristics. The existence of a micelle-vesicle transition in the reconstitution systems led to a decrease in the turnover rate of PMCA by a direct effect on the residence time of the phosphorylated intermediates, suggesting a slower dephosphorylation rate. Otherwise, the marked differences in PMCA *kp* attained in DMPC or DOPC mixed micelles were not due to an effect on the phosphorylated intermediates. We propose here that the location of several positively charged groups within the hydrophobic core, when PMCA was embedded in a DOPC bilayer, may explain the lower turnover rate. We found that the optimum hydrophobic thickness for PMCA is 24 Å, consistent with the maximal Ca^{2+}-ATPase activity.

The Inhibitory Phase—It has been reported that $C_{12}E_{10}$ forms spherical micelles in aqueous solutions (45). When bilayer-forming long-chain lipids are mixed with these detergent molecules, the two components mix to form mixed micelles with a similar size (Fig. 3). However, when these micelles are enriched in lipids, a transition to vesicle may occur, which increases the possibility of aggregates formation (Fig. 3). These aggregates, described as binary, bilayered mixed micelles, are known as bicelles (46). These structures are characterized by the presence of a central portion forming an actual lipid bilayer, surrounded or interspersed with "rims" of detergent molecules (47). This change in organization between lipid and detergent molecules is accompanied by changes in the curvature and an increase in the lateral pressure in the center of the bilayers (48). Such effects may affect folding and conformation of integral membrane proteins (49–51). Accordingly, we show here that in the case of PMCA, Ca^{2+}-ATPase activity decreases to 40% of the maximum level at $X_{DMPC} = 0.7$. In contrast, when mixed micelles are formed with DLPC, Ca^{2+}-ATPase activity decreases at a higher X_{PC}. This might be related with the fact that a higher amount of this phospholipid was necessary to modify the $C_{12}E_{10}$/DLPC particle size (Fig. 3*B*). This phenomenon could be explained by a higher degree of mixing between DLPC and micelles forming species than between these species and DMPC (52).

It has been demonstrated that, after a micelle-vesicle transition, there might be a coexistence of bicelles with vesicles (53, 54). In our system, PMCA may be inserted in a vesicle with its catalytic site facing either the luminal side or the solution. In both cases, the Ca^{2+}-ATPase activity would be impaired by a lack of substrate accessibility or by Ca^{2+} accumulation in the vesicle. Of note, we show here that the decrease of the Ca^{2+}-ATPase activity observed at higher X_{PC} is not due to the vesicle filling with calcium (Fig. 4) or a lack of accessibility to substrates

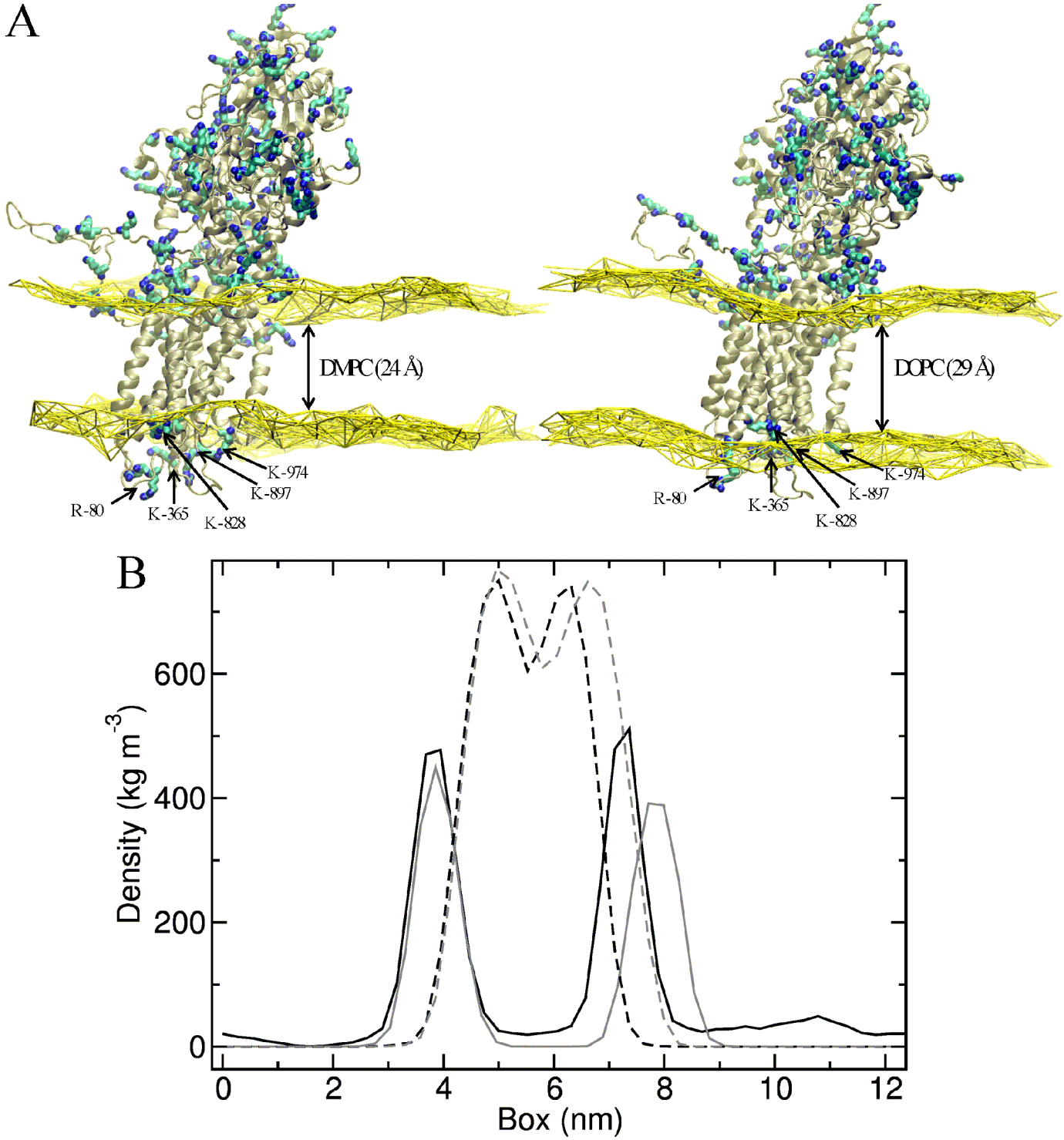

FIGURE 7. **MD simulations of PMCA model in DMPC and DOPC bilayers.** *A*, average of PMCA model structure together with a yellow surface representing the average positions of phosphorus atoms in DMPC (*left*) or DOPC (*right*) bilayer. Lysine (*K*) and arginine (*R*) residues are shown as *cyan* and *blue sticks*. The *arrows* show Arg-80, Lys-365, Lys-828, Lys-897, and Lys-974 residues, located in the PMCA extracellular domain. *B*, density graph of the polar heads and hydrophobic tails. The polar heads of DMPC (*gray*) and DOPC (*black*) are shown in *continuous lines*, and the hydrophobic tails are shown in *dotted lines*.

and/or cofactors (Figs. 4 and 5). Although this result does not fully discard the possibility of a change in the PMCA apparent affinity by Ca^{2+} whenever X_{PC} increases, preliminary studies of our group suggest that PMCA apparent affinity for Ca^{2+} is not modified by reconstitution in $X_{DMPC} = 0.25$ or $X_{DMPC} = 0.7$. On the same subject, PMCA inhibition by higher X_{PC} was similar in the presence of 30 μM or 2 mM ATP (Figs. 6 and 1, respectively), suggesting that the pump affinity for ATP is not modified by an increase in X_{PC}.

Kosk-Kosicka *et al.* (6) have previously described that the addition of neutral phospholipids to a phospholipid-depleted PMCA preparation produces no effect on the steady-state *E*P

level. In contrast, the present work shows that PMCA reconstitution at higher X_{PC} increases the *E*P level concomitantly with a decrease in PMCA turnover (Fig. 6 and Table 2). When a reaction cycle of an enzyme is closed, as in the case of P-ATPases, the sum of the residence times of all intermediaries is equal to the transit time of the enzyme (44). Therefore, if we consider that the transit time increases from 17 ± 1 ms at $X_{DMPC} = 0.25$ to 29 ± 3 ms at $X_{DMPC} = 0.7$, the residence time of one or more intermediates must be changing in about 12 ± 4 ms. Notably, our results show that the time of residence in *E*P (t(*E*P)) increases about 7.4 ± 1.0 ms (from 4.5 ± 0.2 to 11.9 ± 0.8; Table 3) when X_{DMPC} changes from 0.25 to 0.7. These results strongly suggest that the lower PMCA turnover observed at higher X_{PC} is related to an increase of t(*E*P). As we described under "Results," the only possibility that the *E*P level in steady state (and consequently t(*E*P)) can increase along with a decrease of enzyme turnover is if the dephosphorylation rate decreases. Therefore, we suggest that an increase of X_{PC} in PMCA reconstitution medium produces a lower enzyme turnover through a decrease in the rate of dephosphorylation.

It has been described that in addition to being the substrate in the phosphorylation of the E_1Ca state, ATP also functions in a non-phosphorylating mode by enhancing the rates of the steps involved in phosphoenzyme turnover (E_1CaP → E_2P and E_2P → E_2) as well as the $E_2 \rightarrow E_1$Ca transition of the dephosphoenzyme (55). Taking into account that PMCA apparent affinities for ATP in the catalytic and modulatory sites are 25 and 250 μM, respectively (42), results from Fig. 6 suggest that the increase of t(*E*P) could not be due to the absence of the modulatory effect of ATP.

PMCA Activation Phase—Recently, we have used a phospholipid analog ([^{125}I]TID-PC/16) to study the transmembrane domain conformation in SERCA (12), Na/K ATPase (56), and different isoforms of the PMCA (57). Transmembrane domain conformations of these ATPases change during the catalytic cycle, and the amount of annular lipids also varies (*i.e.* the conformational changes that allow the ion transport by these P-ATPases involve changes in the arrangement of lipids surrounding the protein). Regarding E_2 and E_1Ca conformations, we have determined that the number of DMPC molecules directly associated with PMCA transmembrane domain was 19 and 30, respectively (57). Apart from that, Dodes Traian *et al.* (14) combined kinetic and structural information to propose a model in which the enzyme selects a particular lipid microenvironment, and then this lipids produces a conformational change at the transmembrane region, which is further propagated toward the catalytic domain. In this model (Equation 5), the $X_{0.5}$ parameter is related to the degree of lipid coverage of the transmembrane surface, producing half-maximal activation. Accordingly, we would be able to estimate the amount of PC molecules that leads to PMCA maximal activation. If we consider that the $C_{12}E_{10}$ aggregation number does not change at least until $X_{DMPC} = 0.25$, we may propose that the maximal PMCA activation is observed when there exist about 25 molecules of DMPC in the mixed micelle. Note that this consideration may only be valid if the particle size does not vary (as can be seen in Fig. 3 for the mentioned X_{PC} range). In addition, this value turned to be similar for most of the neutral phospholipids assayed (except for DLPC). Remarkably, this number of phospholipid molecules is similar to the amount of DMPC molecules directly associated with the PMCA transmembrane domain (57). Nonetheless, this finding does not necessarily indicate that these 25 molecules of DMPC may be directly associated with the protein.

The activating effect of different phospholipids was also investigated in other P-type ATPases. SERCA displays maximum activity when embedded in bilayers with a thickness around 30 Å (58). The chain length dependence of the activity of the Na^+/K^+-ATPase is slightly different from that of SERCA, with an optimum chain length of C22 in the absence of cholesterol and C18 in its presence (16). Here we show that Ca^{2+}-ATPase activity is maximal in the presence of a DMPC bilayer (*i.e.* a hydrophobic thickness of about 24 Å). In agreement with our results for PMCA, the reconstitution of SERCA (43) and Na^+/K^+-ATPase (16) in bilayers whose thickness differs from the optimal results in a decrease in the turnover of the enzyme(s). In SERCA, this was attributed to an increase of the *E*P level in steady state produced by a decrease of the dephosphorylation rate (43). On the contrary, our results show that DOPC produces a decrease in *E*P level with respect to DMPC without changes in the residence time in *E*P. This result was similar for higher X_{PC}, suggesting that the increase of t(*E*P) is related to the physical state of the micelles or bicelles and not to changes in the bilayer thickness. In agreement with these findings, Sonntag *et al.* (15) suggested that a change in the bilayers hydrophobic thickness in SERCA may have a direct effect on the conformational change between the E_1 and E_2 states.

MD simulations revealed that the upper layers of DMPC and DOPC adapt to interact with the positive charges of the large number of Lys residues that are located near the interface (Fig. 7*A*). However, the lower layer of the DOPC bilayer leaves several positively charged groups within the hydrophobic core, whereas in the presence of DMPC membranes, these residues are placed in a more polar environment, interacting with phosphorus atoms or exposed to the solvent. It is notable that these simulations were carried out in the absence of detergent, contrasting with the reconstitution systems used in our experiments. Although the detergent molecules would probably increase the membrane fluidity, it has been demonstrated that the thickness of a bilayer composed of $C_{12}E_8$ and DOPC (in a ratio of 30:80 (*i.e.* an X_{PC} of about 0.3)) remained nearly constant with respect to a pure phospholipid (15). Importantly, the protein structure was only slightly affected by the detergent environment, consistent with its functional integrity. Taking this evidence into account, we propose that the lower Ca^{2+}-ATPase activity found in $X_{DOPC} = 0.3$ could be a direct consequence of the apparent hydrophobic mismatch produced by a thicker bilayer. This effect was also observed at higher X_{PC}, where Ca^{2+}-ATPase activity is lower in DOPC with respect to DMPC (Fig. 1). As a whole, in the presence of a higher X_{DOPC}, the decrease in turnover rate would be due not only to an increase in t(*E*P) (Table 3) but also to the hydrophobic mismatch (Fig. 7).

An important difference between SERCA and PMCA is that the latter is activated by calmodulin and acidic phospholipids (11, 59). PMCA activation by these modulators involves confor-

mational changes that, among other changes, modify the accessible area to lipids of the transmembrane domain (60). The acidic phospholipid binding region is a basic sequence enriched in Lys residues, located near the lipid/water interface of the first cytosolic loop (61). Thus, considering the higher density of Lys residues in the acidic phospholipid region near the interface, it is possible that PMCA has a more stringent optimum thickness with respect to SERCA and Na/K-ATPase. In other words, this region has structural effects that may favor a narrow hydrophobic thickness for PMCA. If we consider that the secondary structure of the helices mostly does not change, it is clear that the transmembrane helices should adopt various tilt angles, depending on the mismatch (62), producing a higher protein-lipid interaction. On this subject, Mitra *et al.* (63) showed that, although the average thickness of biological membranes is 30 Å, variations up to 5 Å arise when protein is inserted in these membranes. Therefore, it could be possible that in a physiological condition, PMCA causes a thickness decrease in its environment that leads to its optimum activity. In conclusion, differential modulation by neutral phospholipids could be a general mechanism for regulating membrane protein function.

Acknowledgments—We are indebted to Drs. Rolando C. Rossi, Joshua R. Berlin, and Mariela Ferreira-Gomes (Universidad de Buenos Aires) for helpful comments and to Fundosol (Argentina) for kindly providing the human blood.

REFERENCES

1. Strehler, E. E., Caride, A. J., Filoteo, A. G., Xiong, Y., Penniston, J. T., and Enyedi, A. (2007) Plasma membrane Ca^{2+} ATPases as dynamic regulators of cellular calcium handling. *Ann. N.Y. Acad. Sci.* **1099,** 226–236
2. Rega, A., and Garrahan, P. J. (1986) *The Ca^{2+} Pump of Plasma Membranes*, pp. 115–125, CRC Press, Boca Raton, FL
3. Lee, A. G. (2011) Biological membranes: the importance of molecular detail. *Trends Biochem. Sci.* **36,** 493–500
4. Adamian, L., Naveed, H., and Liang, J. (2011) Lipid-binding surfaces of membrane proteins: evidence from evolutionary and structural analysis. *Biochim. Biophys. Acta* **1808,** 1092–1102
5. Lee, A. G. (2003) Lipid-protein interactions in biological membranes: a structural perspective. *Biochim. Biophys. Acta* **1612,** 1–40
6. Kosk-Kosicka, D. (1990) Comparison of the red blood cell Ca^{2+}-ATPase in ghost membranes and after purification. *Mol. Cell Biochem.* **99,** 75–81
7. Carafoli, E. (1994) Biogenesis: plasma membrane calcium ATPase: 15 years of work on the purified enzyme. *FASEB J.* **8,** 993–1002
8. Levi, V., Rossi, J. P. F. C., Echarte, M. M., Castello, P. R., and González Flecha, F. L. (2000) Thermal stability of the plasma membrane calcium pump: quantitative analysis of its dependence on lipid-protein interactions. *J. Membr. Biol.* **173,** 215–225
9. Ronner, P., Gazzotti, P., and Carafoli, E. (1977) A lipid requirement for the (Ca^{2+} + Mg^{2+})-activated ATPase of erythrocyte membranes. *Arch. Biochem. Biophys.* **179,** 578–583
10. Niggli, V., Adunyah, E. S., and Carafoli, E. (1981) Acidic phospholipids, unsaturated fatty acids, and limited proteolysis mimic the effect of calmodulin on the purified erythrocyte Ca^{2+}-ATPase. *J. Biol. Chem.* **256,** 8588–8592
11. Filomatori, C. V., and Rega, A. F. (2003) On the mechanism of activation of the plasma membrane Ca^{2+}-ATPase by ATP and acidic phospholipids. *J. Biol. Chem.* **278,** 22265–22271
12. Mangialavori, I., Villamil Giraldo, A. M., Marino Buslje, C., Ferreira Gomes, M., Caride, A. J., and Rossi, J. P. F. C. (2009) A new conformation in sarcoplasmic reticulum calcium pump and plasma membrane Ca^{2+} pumps revealed by a photoactivatable phospholipidic probe. *J. Biol. Chem.* **284,** 4823–4828
13. Mangialavori, I. C., Ferreira-Gomes, M. S., Saffioti, N. A., González-Lebrero, R. M., Rossi, R. C., and Rossi, J. P. F. C. (2013) Conformational changes produced by ATP binding to the plasma membrane calcium pump. *J. Biol. Chem.* **288,** 31030–31041
14. Dodes Traian, M. M., Cattoni, D. I., Levi, V., and González Flecha, F. L. (2012) A two-stage model for lipid modulation of the activity of integral membrane proteins. *PLoS One* **7,** e39255
15. Sonntag, Y., Musgaard, M., Olesen, C., Schiøtt, B., Møller, J. V., Nissen, P., and Thøgersen, L. (2011) Mutual adaptation of a membrane protein and its lipid bilayer during conformational changes. *Nat. Commun.* **2,** 304
16. Cornelius, F. (2001) Modulation of Na,K-ATPase and Na-ATPase activity by phospholipids and cholesterol. I. Steady-state kinetics. *Biochemistry* **40,** 8842–8851
17. Lee, A. G. (2011) Lipid-protein interactions. *Biochem. Soc. Trans.* **39,** 761–766
18. Strehler, E. E., James, P., Fischer, R., Heim, R., Vorherr, T., Filoteo, A. G., Penniston, J. T., and Carafoli, E. (1990) Peptide sequence analysis and molecular cloning reveal two calcium pump isoforms in the human erythrocyte membrane. *J. Biol. Chem.* **265,** 2835–2842
19. Niggli, V., Penniston, J. T., and Carafoli, E. (1979) Purification of the (Ca^{2+}-Mg^{2+})-ATPase from human erythrocyte membranes using a calmodulin affinity column. *J. Biol. Chem.* **254,** 9955–9958
20. Chen, P. S., Toribara, T. Y., and Warner, H. (1956) Microdetermination of phosphorus. *Anal. Chem.* **28,** 1756–1758
21. Fiske, C. H., and Subbarow, Y. (1925) The colorimetric determination of phosphorus. *J. Biol. Chem.* **66,** 375–400
22. Richards, D. E., Rega, A. F., and Garrahan, P. J. (1978) Two classes of site for ATP in the Ca^{2+}-ATPase from human red cell membranes. *Biochim. Biophys. Acta* **511,** 194–201
23. Culbertson, C. T., Jacobson, S. C., and Michael Ramsey, J. (2002) Diffusion coefficient measurements in microfluidic devices. *Talanta* **56,** 365–373
24. Haustein, E., and Schwille, P. (2003) Ultrasensitive investigations of biological systems by fluorescence correlation spectroscopy. *Methods* **29,** 153–166
25. Echarte, M. M., Levi, V., Villamil, A. M., Rossi, R. C., and Rossi, J. P. F. C. (2001) Quantitation of plasma membrane calcium pump phosphorylated intermediates by electrophoresis. *Anal. Biochem.* **289,** 267–273
26. Penniston, J. T., Padányi, R., Pászty, K., Varga, K., Hegedus, L., and Enyedi, A. (2014) Apart from its known function, the plasma membrane Ca^{2+}-ATPase can regulate Ca^{2+} signaling by controlling phosphatidylinositol 4,5-bisphosphate levels. *J. Cell Sci.* **127,** 72–84
27. Van Der Spoel, D., Lindahl, E., Hess, B., Groenhof, G., Mark, A. E., and Berendsen, H. J. C. (2005) GROMACS: fast, flexible, and free. *J. Comput. Chem.* **26,** 1701–1718
28. Schmidt, T. H., and Kandt, C. (2012) LAMBADA and InflateGRO2: efficient membrane alignment and insertion of membrane proteins for molecular dynamics simulations. *J. Chem. Inf. Model.* **52,** 2657–2669
29. Feenstra, K. A., Hess, B., and Berendsen, H. J. C. (1999) Improving efficiency of large time-scale molecular dynamics simulations of hydrogen-rich systems. *J. Comput. Chem.* **20,** 786–798
30. Almog, S., Litman, B. J., Wimley, W., Cohen, J., Wachtel, E. J., Barenholz, Y., Ben-Shaul, A., and Lichtenberg, D. (1990) States of aggregation and phase transformations in mixtures of phosphatidylcholine and octyl glucoside. *Biochemistry* **29,** 4582–4592
31. Jackson, M. L., Schmidt, C. F., Lichtenberg, D., Litman, B. J., and Albert, A. D. (1982) Solubilization of phosphatidylcholine bilayers by octyl glucoside. *Biochemistry* **21,** 4576–4582
32. Levy, D., Gulik, A., Seigneuret, M., and Rigaud, J. L. (1990) Phospholipid vesicle solubilization and reconstitution by detergents: symmetrical analysis of the two processes using octaethylene glycol mono-*N*-dodecyl ether. *Biochemistry* **29,** 9480–9488
33. Paternostre, M. T., Roux, M., and Rigaud, J. L. (1988) Mechanisms of membrane protein insertion into liposomes during reconstitution procedures involving the use of detergents. 1. Solubilization of large unilamellar liposomes (prepared by reverse-phase evaporation) by Triton X-100, octyl glucoside, and sodium cholate. *Biochemistry* **27,** 2668–2677
34. Lichtenberg, D. (1985) Characterization of the solubilization of lipid bi-

layers by surfactants. *Biochim. Biophys. Acta* **821,** 470–478
35. Silvius, J. R. (1992) Cholesterol modulation of lipid intermixing in phospholipid and glycosphingolipid mixtures: evaluation using fluorescent lipid probes and brominated lipid quenchers. *Biochemistry* **31,** 3398–3408
36. Erdahl, W. L., Chapman, C. J., Taylor, R. W., and Pfeiffer, D. R. (1994) Ca^{2+} transport properties of ionophores A23187, ionomycin, and 4-BrA23187 in a well defined model system. *Biophys. J.* **66,** 1678–1693
37. Pressman, B. C. (1976) Biological applications of ionophores. *Annu. Rev. Biochem.* **45,** 501–530
38. Sarkadi, B., Enyedi, A., Földes-Papp, Z., and Gárdos, G. (1986) Molecular characterization of the *in situ* red cell membrane calcium pump by limited proteolysis. *J. Biol. Chem.* **261,** 9552–9557
39. Reed, P. W., and Lardy, H. A. (1972) A23187: a divalent cation ionophore. *J. Biol. Chem.* **247,** 6970–6977
40. Luterbacher, S., and Schatzmann, H. J. (1983) The site of action of La^{3+} in the reaction cycle of the human red cell membrane Ca^{2+}-pump ATPase. *Experientia* **39,** 311–312
41. Herscher, C. J., and Rega, A. F. (1996) Pre-steady-state kinetic study of the mechanism of inhibition of the plasma membrane Ca^{2+}-ATPase by lanthanum. *Biochemistry* **35,** 14917–14922
42. Echarte, M. M., Rossi, R. C., and Rossi, J. P. F. C. (2007) Phosphorylation of the plasma membrane calcium pump at high ATP concentration: on the mechanism of ATP hydrolysis. *Biochemistry* **46,** 1034–1041
43. Starling, A. P., East, J. M., and Lee, A. G. (1995) Effects of phospholipid fatty acyl chain length on phosphorylation and dephosphorylation of the Ca^{2+}-ATPase. *Biochem. J.* **310,** 875–879
44. Sines, J. J., and Hackney, D. D. (1987) A residence-time analysis of enzyme kinetics. *Biochem. J.* **243,** 159–164
45. Warisnoicharoen, W., Lansley, A. B., and Lawrence, M. J. (2000) Light scattering investigations on dilute nonionic oil-in-water microemulsions. *AAPS PharmSci* **2,** E12
46. Müller, K. (1981) Structural dimorphism of bile salt/lecithin mixed micelles. A possible regulatory mechanism for cholesterol solubility in bile? X-ray structural analysis. *Biochemistry* **20,** 404–414
47. Dürr, U. H. N., Soong, R., and Ramamoorthy, A. (2013) When detergent meets bilayer: birth and coming of age of lipid bicelles. *Prog. Nucl. Magn. Reson. Spectrosc.* **69,** 1–22
48. Seigneuret, M., and Rigaud, J.-L. (1985) Use of the fluorescent pH probe pyranine to detect heterogeneous directions of proton movement in bacteriorhodopsin reconstituted large liposomes. *FEBS Lett.* 10.1016/0014-5793(85)80883-8
49. Booth, P. J., Riley, M. L., Flitsch, S. L., Templer, R. H., Farooq, A., Curran, A. R., Chadborn, N., and Wright, P. (1997) Evidence that bilayer bending rigidity affects membrane protein folding. *Biochemistry* **36,** 197–203
50. Curran, A. R., Templer, R. H., and Booth, P. J. (1999) Modulation of folding and assembly of the membrane protein bacteriorhodopsin by intermolecular forces within the lipid bilayer. *Biochemistry* **38,** 9328–9336
51. Roman, E. A., and González Flecha, F. L. (2014) Kinetics and thermodynamics of membrane protein folding. *Biomolecules* **4,** 354–373
52. Lind, J., Nordin, J., and Mäler, L. (2008) Lipid dynamics in fast-tumbling bicelles with varying bilayer thickness: effect of model transmembrane peptides. *Biochim. Biophys. Acta* **1778,** 2526–2534
53. Vinson, P. K., Talmon, Y., and Walter, A. (1989) Vesicle-micelle transition of phosphatidylcholine and octyl glucoside elucidated by cryo-transmission electron microscopy. *Biophys. J.* **56,** 669–681
54. Edwards, K., Almgren, M., Bellare, J., and Brown, W. (1989) Effects of Triton X-100 on sonicated lecithin vesicles. *Langmuir* **5,** 473–478
55. Jensen, A.-M. L., Sørensen, T. L.-M., Olesen, C., Møller, J. V., and Nissen, P. (2006) Modulatory and catalytic modes of ATP binding by the calcium pump. *EMBO J.* **25,** 2305–2314
56. Mangialavori, I., Montes, M. R., Rossi, R. C., Fedosova, N. U., and Rossi, J. P. F. C. (2011) Dynamic lipid-protein stoichiometry on E1 and E2 conformations of the Na^+/K^+-ATPase. *FEBS Lett.* **585,** 1153–1157
57. Mangialavori, I. C., Corradi, G., Rinaldi, D. E., de la Fuente, M. C., Adamo, H. P., and Rossi, J. P. F. C. (2012) Autoinhibition mechanism of the plasma membrane calcium pump isoforms 2 and 4 studied through lipid-protein interaction. *Biochem. J.* **443,** 125–131
58. Starling, A. P., East, J. M., and Lee, A. G. (1993) Effects of phosphatidylcholine fatty acyl chain length on calcium binding and other functions of the calcium-magnesium-ATPase. *Biochemistry* **32,** 1593–1600
59. Falchetto, R., Vorherr, T., and Carafoli, E. (1992) The calmodulin-binding site of the plasma membrane Ca^{2+} pump interacts with the transduction domain of the enzyme. *Protein Sci.* **1,** 1613–1621
60. Mangialavori, I., Villamil-Giraldo, A. M., Pignataro, M. F., Ferreira-Gomes, M., Caride, A. J., and Rossi, J. P. F. C. (2011) Plasma membrane calcium pump (PMCA) differential exposure of hydrophobic domains after calmodulin and phosphatidic acid activation. *J. Biol. Chem.* **286,** 18397–18404
61. Pinto, F. de T., and Adamo, H. P. (2002) Deletions in the acidic lipid-binding region of the plasma membrane Ca^{2+} pump: a mutant with high affinity for Ca^{2+} resembling the acidic lipid-activated enzyme. *J. Biol. Chem.* **277,** 12784–12789
62. Kandasamy, S. K., and Larson, R. G. (2006) Molecular dynamics simulations of model trans-membrane peptides in lipid bilayers: a systematic investigation of hydrophobic mismatch. *Biophys. J.* **90,** 2326–2343
63. Mitra, K., Ubarretxena-Belandia, I., Taguchi, T., Warren, G., and Engelman, D. M. (2004) Modulation of the bilayer thickness of exocytic pathway membranes by membrane proteins rather than cholesterol. *Proc. Natl. Acad. Sci. U.S.A.* **101,** 4083–4088